

Experimental Report:

Direct evaluation of measurement uncertainties by feedback compensation in neutron interferometry

1 Motivation

We investigate the which-path problem of a neutron moving through a two-path interferometer. We use a description which distinguishes between collective path probabilities p and individual path occupations ω . While the former describe a situation where e.g. 80% of the neutrons take one path and 20% take the other path, the latter describe the case where a single neutron occupies e.g. one path to 66.6% and the other path to 33.3%. We will show first, that this model reproduces the expected overall statistics, and second, that we can distinguish experimentally between the two cases using the so-called *feedback compensation* scheme (see¹ for LATEX document and figures).

In the experiment, proposed in [1], a spin rotation by a sufficiently small angle α is applied in path I of a two path interferometer (see Fig. 1). A neutron moving along path I has $\omega_I = 1$ and $\omega_{II} = 0$ and experiences a spin rotation of exactly $\omega_I \times \alpha = \alpha$. In our interferometer we use an asymmetric beam splitter with an intensity ratio 1:4 which creates the input state

$$|\psi\rangle = \frac{2}{\sqrt{5}}|I\rangle + \frac{1}{\sqrt{5}}|II\rangle.$$

If we perform a **which-path** measurement by inserting a detector in path I or II respectively we obtain $p(I) = 0.8$ and $p(II) = 0.2$, i. e., an 80 % chance to find the neutron in the path with the spin rotation. The roman numbers in parenthesis denote the position of the detector. The average spin rotation is given by

$$p(I) \times (\omega_I(I) \times \alpha) + p(II) \times (\omega_I(II) \times \alpha) = 0.8 \times \alpha := \omega_{I\text{av}} \times \alpha$$

and allows to infer the *input path distribution*, i.e. the factor 0.8. However, we know that this is only an average of the real spin rotations of $1 \times \alpha$ and $0 \times \alpha$. If we perform an **interference measurement** in

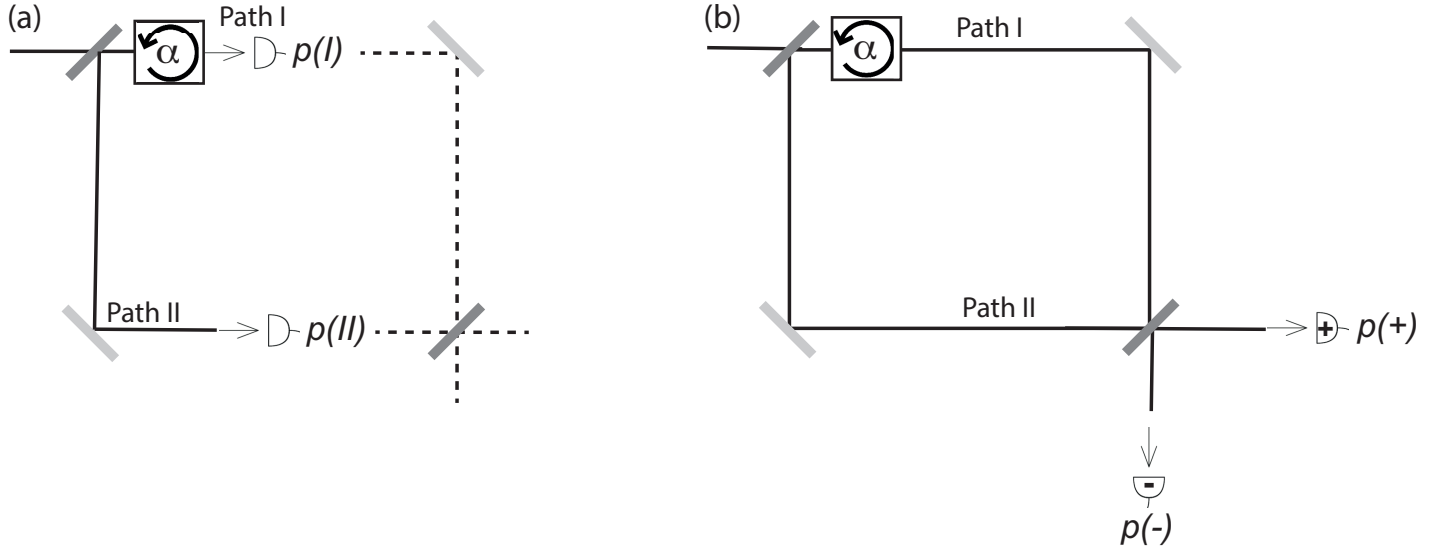


Figure 1: Uncompensated interferometer scheme for (a) *which-path* and (b) *interference* measurements.

¹<https://www.overleaf.com/read/rwtsqfwfvqs>

the output ports of the interferometer, the outcome probabilities are $p(+) = 0.9$ in the forward output port (where we have constructive interference) and $p(-) = 0.1$ in the side output port (where we have destructive interference). The spin rotations in the two output ports are $\frac{2}{3} \times \alpha := \omega_I(+)\times\alpha$ for constructive interference and $2 \times \alpha := \omega_I(-)\times\alpha$ for destructive interference. Again, the input path distribution is reproduced by the statistics of the two outcomes,

$$p(+) \times \omega_I(+)\times\alpha + p(-) \times \omega_I(-)\alpha = 0.8 \times \alpha = \omega_{Iav} \times \alpha.$$

We conclude that the *path distribution* of the input state is equally described by two different *probability distributions*, selected by the choice of output measurement, i.e., the *measurement context*.

It is also possible to compare the *path occupation uncertainties* resulting from the two probability distributions: in the **which-path** experiment, mixing the paths results corresponds to an occupation uncertainty of

$$p(I) \times [\underbrace{(\omega_I(I) - \omega_{Iav}) \times \alpha^2}_{0.2}] + p(II) \times [\underbrace{(\omega_I(II) - \omega_{Iav}) \times \alpha^2}_{-0.8}] = 0.16 \times \alpha^2 := \Delta\omega_I^2 \times \alpha^2.$$

Mixing the interferometer outputs in the **interferences measurement**, results in the same amount of uncertainty

$$p(+) \times [\underbrace{(\omega_I(+)-\omega_{Iav}) \times \alpha^2}_{-1.3}] + p(-) \times [\underbrace{(\omega_I(-)-\omega_{Iav}) \times \alpha^2}_{1.2}] = 0.16 \times \alpha^2 = \Delta\omega_I^2 \times \alpha^2.$$

Both probability distributions (*mixing effects*) induce a reduction of the *polarization fringe visibility* $\propto \Delta\omega_I^2 \times \alpha^2$. On the other hand, the expected *path occupation uncertainty* I , in terms of standard deviations of the projector onto path I , denoted as $\hat{\Pi}_I$, in state $|\psi\rangle$, is given by

$$\Delta\omega_I^2 = \langle\psi|\hat{\Pi}_I^2|\psi\rangle - \langle\psi|\hat{\Pi}_I|\psi\rangle^2 = 0.16.$$

The same which-path uncertainty $\Delta\omega_I$ of the input state appears in both the which-path measurement and in the interference measurement.

Feedback compensation is a method to determine both the angle of spin rotation and its fluctuations. The scheme is illustrated in Fig. 2. If the angle does not fluctuate, every neutron spin must have rotated

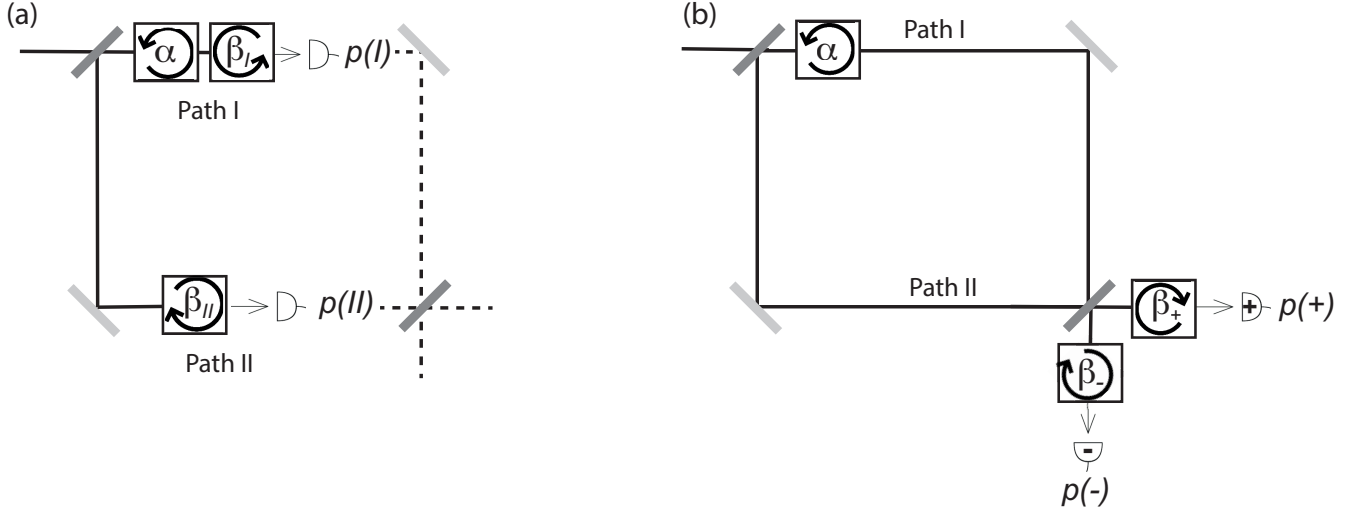


Figure 2: Compensated interferometer scheme for (a) *which-path* and (b) *interference measurements*.

by the same angle. Hence, the angle of rotation of each particle depends on the path occupation of the particle, and the rotation angle is a reliable record of the precise path occupation, even if it takes values other than zero or one. As before, the spin is rotated in path I by the angle α . In the output port the spin is then rotated by β . We determine the output spin polarization

$$\langle \hat{\sigma}_x \rangle(\beta) = V \cos(\beta + \omega_I \times \alpha)$$

as a function of β , where ω_I expresses the average presence of the neutron in path I and the visibility V determines the uncertainty of this average as

$$V \approx 1 - \frac{1}{2} \Delta\omega_I^2 \alpha^2,$$

with expected path uncertainty of $\Delta\omega_I^2 = \langle \psi | \hat{\Pi}_I^2 | \psi \rangle - \langle \psi | \hat{\Pi}_I | \psi \rangle^2 = 0.16$, from before.

For the **which-path** context we get the following observable fringes

$$\begin{aligned} \langle \hat{\sigma}_x \rangle(\beta|I) &= \cos(\omega_I(I) \times \alpha + \beta) \\ \langle \hat{\sigma}_x \rangle(\beta|II) &= \cos(\omega_I(II) \times \alpha + \beta), \end{aligned} \quad (1)$$

with $\omega_I(I) = 1$ and $\omega_I(II) = 0$, while for the **interference** context we get

$$\begin{aligned} \langle \hat{\sigma}_x \rangle(\beta|+) &= \cos(\omega_I(+) \times \alpha + \beta) \\ \langle \hat{\sigma}_x \rangle(\beta|-) &= \cos(\omega_I(-) \times \alpha + \beta), \end{aligned} \quad (2)$$

with $\omega_I(+) = 2/3$ and $\omega_I(-) = 2$. A visibility of $V = 1$ of the fringes $\langle \hat{\sigma}_x \rangle(\beta)$ therefore indicates an exact path value ω_I , even if this value is different from 0 or 1. ω_I is determined experimentally by scanning β and maximizing $\langle \hat{\sigma}_x \rangle(\beta)$.

Again the path context and the interference context express the same which-path fluctuation, which is confirmed by taking the average of the two fringes using the probabilities:

$$\begin{aligned} \langle \hat{\sigma}_x \rangle(\beta) &= p(I) \cos(\omega_I(I) \times \alpha + \beta) + p(II) \cos(\omega_I(II) \times \alpha + \beta) \\ &\approx p(+) \cos(\omega_I(+) \times \alpha + \beta) + p(-) \cos(\omega_I(-) \times \alpha + \beta), \end{aligned} \quad (3)$$

with $p(I) = 0.8$, $p(II) = 0.2$, $p(+) = 0.9$, $p(-) = 0.1$, $\omega_I(I) = 1$, $\omega_I(II) = 0$, $\omega_I(+) = 2/3$ and $\omega_I(-) = 2$.

In summary, the multiple of α , by which the β -fringes are shifted, reveal the path occupation (presence of the neutron in the path); in the *which path* measurement we get $\omega(I) = 1$ or $\omega(II) = 0$ with probabilities $p(I) = 0.8$ and $p(II) = 0.2$. For the interference measurement, this presence is $\omega_I(+) = 2/3$ at a probability of $p(+) = 0.9$ and $\omega_I(-) = 2$ at a probability of $p(-) = 0.1$. Both values are *uncertainty free* ($V = 1$), indicating that each and every neutron is distributed between the paths in the same manner.

2 Experimental Scheme & Realization

In our neutron interferometric [2, 3] experiment, based on a proposed scheme from [1] and schematically illustrated in Fig. 3, the *system* state $\hat{\rho}_S$ is represented by the two *path* eigenstates in the neutron interferometer, denoted as $|P_z; +\rangle := |I\rangle$ and $|P_z; -\rangle := |II\rangle$, for path I and II , respectively. The *probe* qubit is represented by the neutron's spin 1/2 two-level system, with eigenstates $|S_z; \pm\rangle$ in respect to the quantization axis z , and initially prepared as $|S_i\rangle = |S_x; +\rangle = 1/\sqrt{2}(|S_z; +\rangle + |S_z; -\rangle)$. In order to obtain a real weak value the initial (system) state is prepared as

$$\hat{\rho}_S = |\psi\rangle\langle\psi| \text{ with } |\psi\rangle = \frac{2}{\sqrt{5}}|P_z; +\rangle + \frac{1}{\sqrt{5}}|P_z; -\rangle, \quad (4)$$

by a 80:20 beam splitter ($\langle\psi|\hat{\Pi}_I|\psi\rangle = 0.8$ & $\langle\psi|\hat{\Pi}_{II}|\psi\rangle = 0.2$). The initial state of the composite quantum system is given by $\hat{\rho}_{\text{tot}} = \hat{\rho}_S \otimes |S_x; +\rangle\langle S_x; +|$. In that case, the 50:50 (second) beam splitter has output probabilities of 90 percent for constructive interference (+) and 10 percent for destructive interference (-), when the state of the system is projective onto $|m_{\pm}\rangle = |P_x; \pm\rangle$, that is an equally weighted superposition, denoted as

$$|m_{\pm}\rangle = |P_x; \pm\rangle = \frac{1}{\sqrt{2}}(|P_z; +\rangle \pm |P_z; -\rangle). \quad (5)$$

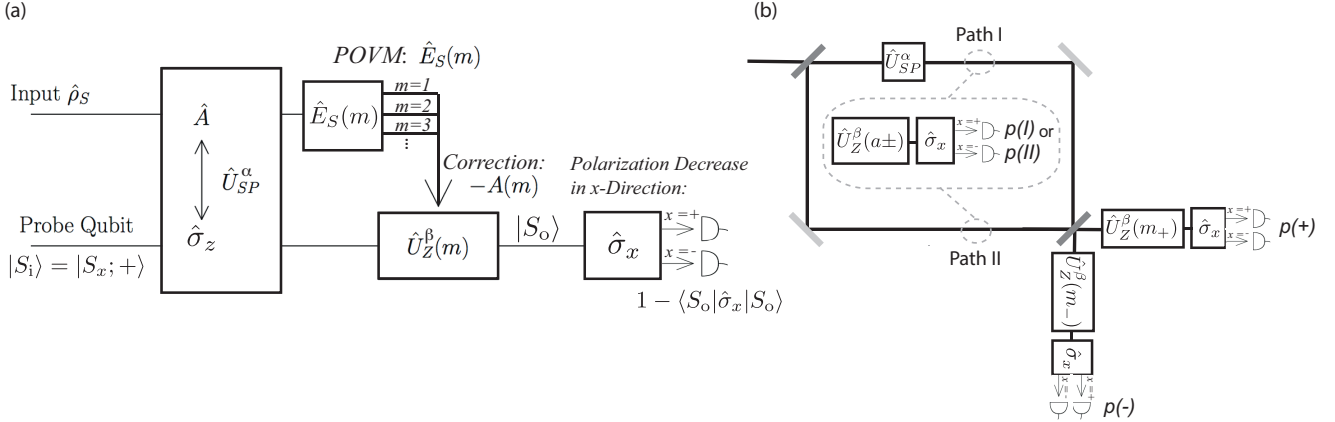


Figure 3: (a) General scheme for feedback compensation from [1]; after a coupling \hat{U}_{SP} between object and probe system, a correction, dependent on POVM measurement results m in input state $\hat{\rho}_S$, is applied. Resulting in suppressed decoherence $D = 1 - \langle \hat{\sigma}_x \rangle$ in probe qubit is. (b) Feedback compensation applied in interferometer scheme for *which-path* and *interference measurement contexts*.

In this Section we present a possible interferometric procedure for feedback compensation by coupling the neutron's spin weakly to its spatial degree of freedom in a single-neutron interferometer setup. The coupling is given by

$$\hat{U}_{SP}^{\alpha} = e^{-i/\hbar \int \hat{H}_{\text{int}} dt} = \exp(-i\frac{\alpha}{2}\Pi_I \otimes \sigma_z),$$

with interaction Hamiltonian $\hat{H}_{\text{int}} = -\vec{\mu} \cdot \vec{B} \hat{\Pi}_I$, where $\hat{\Pi}_I$ (or $\hat{\Pi}_{z\pm}^{(p)}$) is the projection operators on the path eigenstates $|P_z; +\rangle := |I\rangle$ and $\vec{\mu}$ is the neutron's magnetic moment and $\vec{B} = (0, 0, B_z)$ an applied (static) magnetic field. The angle of rotation α is given by $-2\mu B_z \tau / \hbar$, where τ is the neutron's transit time in the magnetic field region. Here, α is the relevant parameter for the *interaction strength* of the measurement. In the actual experimental realization the initial (system) state is prepared as $\hat{\rho}_S = |\psi(\chi, \gamma)\rangle\langle\psi(\chi, \gamma)|$ with

$$|\psi(\chi, \gamma)\rangle = \cos \frac{\gamma}{2}|P_z; +\rangle + e^{i\chi} \sin \frac{\gamma}{2}|P_z; -\rangle$$

where χ is the relative phase between the eigenstates, adjusted by a phase shifter, and γ the relative weight, adjusted by an absorber, which together with the first plate of the interferometer acts like a tunable beam splitter. To get our initial state from Eq.(4), we have to set $\chi = 0$ and $\gamma = \gamma_0 := \text{ArcCos}((\frac{2}{\sqrt{5}})^2 - (\frac{1}{\sqrt{5}})^2) = \text{ArcCos}(\frac{3}{5})$. Behind the interferometer a *correction operation*, denoted as $\hat{U}_z^\beta(m) = A(m)$ (a rotation of $-\beta$ about the z-axis dependent on the results of m) is performed. A spin rotation of $\alpha = \pi/4$ in path I reduces the fringe visibility of the path interference ν from $\nu(\alpha = 0) = 0.8$ to $\nu(\alpha = \pi/4) = 0.739104$. This is a reduction of a factor of 0.92388, which is $\cos(\alpha/2)$, as seen from $I_0 = \frac{1}{2}(1 + \cos \frac{\alpha}{2} \cos \chi \sin \gamma_0)$ (see Appendix B for details of theory curves).

3 Experimental Results

3.1 Which-path context

If the value of $\hat{A} = \hat{\Pi}_I$, i.e., the projector onto path I , is determined after the interaction, feedback can compensate the fluctuating force and undo the decoherence, which is schematically illustrated in Fig. 4(a). Experimentally the projector $\hat{A} = \hat{\Pi}_{I(II)}$, is achieved by blocking path II(I) - see Fig. 4(b). The obtained results of which-path measurements are plotted in Fig. 5 for $\alpha = \pi/4$. Red line indicates the reduced

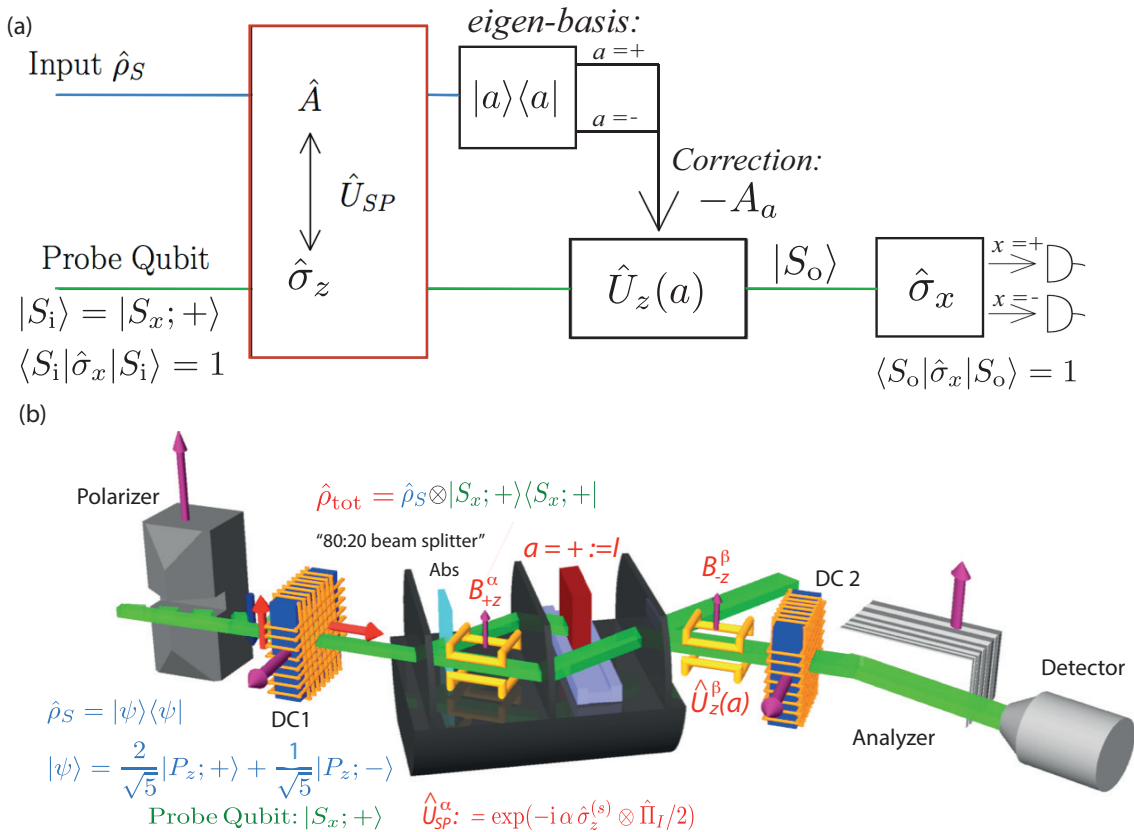


Figure 4: (a) Schematic illustration of feedback compensation of the decoherence in a probe qubit, where the value of \hat{A} is determined after the interaction (*which-way measurement context*). (b) Respective neutron interferometric setup.

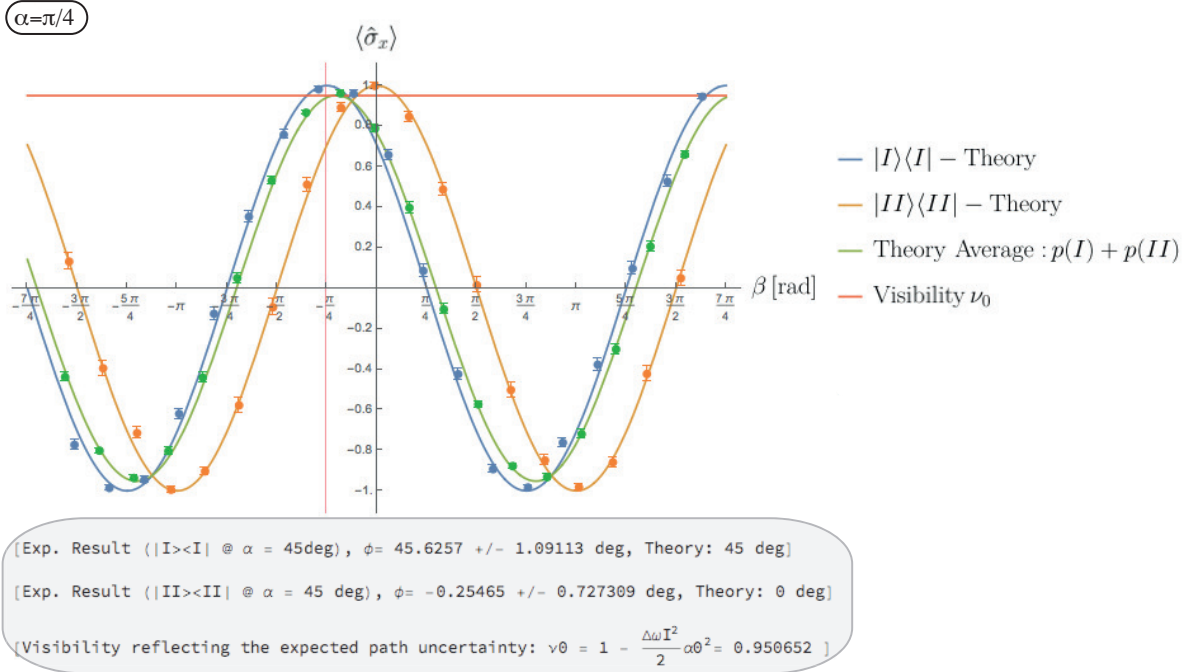


Figure 5: Experimental results of feedback compensation of the decoherence in a probe qubit, where the value of \hat{A} is determined after the interaction (*which-way measurement context*), for interaction strength $\alpha = \pi/4$.

visibility of $\nu(\alpha) \sim \nu_0 - \frac{1}{2}\alpha^2\Delta^2(\hat{\Pi}_I)$, with path uncertainty $\Delta\omega_I^2 = \langle\psi|\hat{\Pi}_I^2|\psi\rangle - \langle\psi|\hat{\Pi}_I|\psi\rangle^2 = 0.16$.

Next the interaction strength is halved to $\alpha = \pi/8$, which is plotted in Fig. 6 and then halved again to

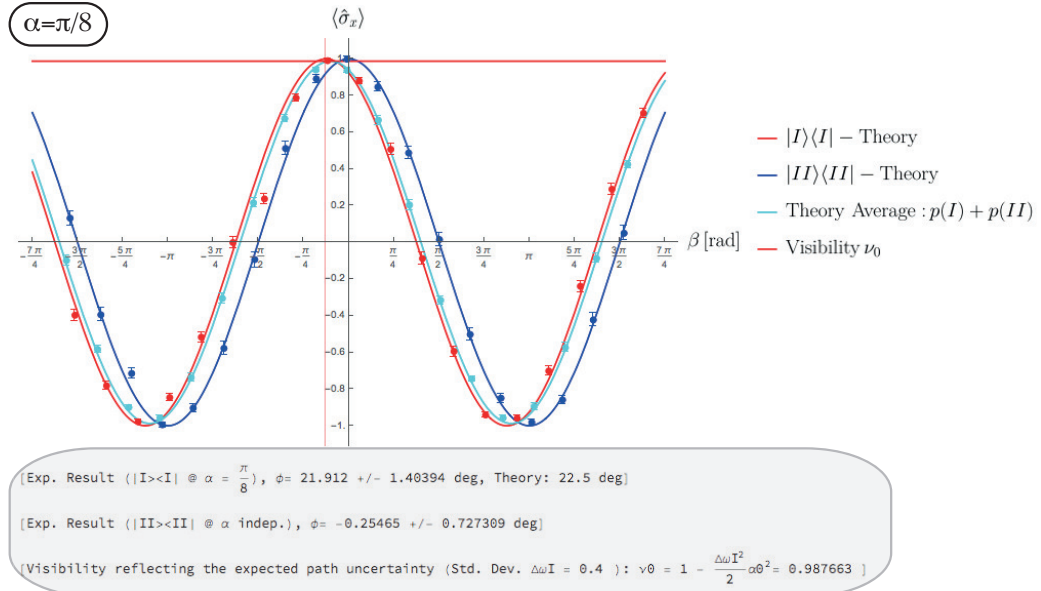


Figure 6: Experimental results of *which-way measurement context*, for interaction strength $\alpha = \pi/8$.

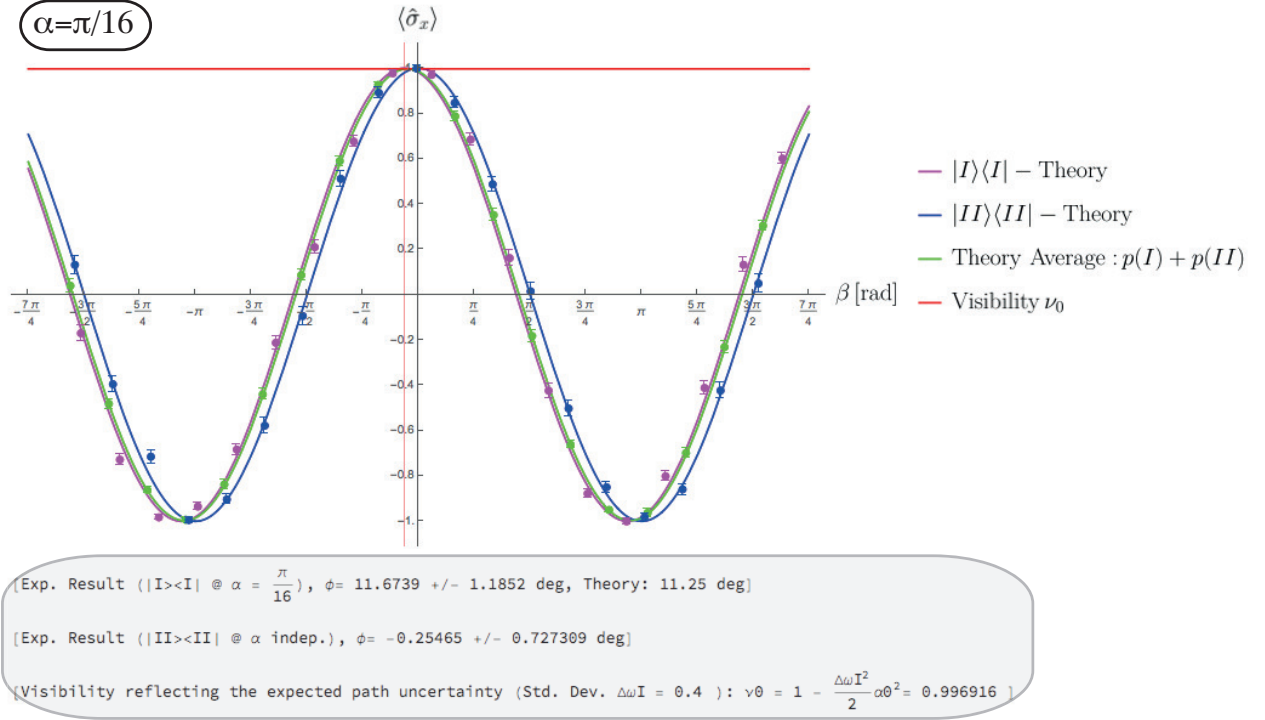


Figure 7: Experimental results of *which-way measurement context*, for interaction strength $\alpha = \pi/16$.

$\alpha = \pi/16$, which is plotted in Fig. 7. The experimentally observed phase shifts ϕ reproduce the theoretically predicted values, given by

$$\begin{aligned}\langle \hat{\sigma}_x \rangle(\beta|I) &= \cos(\omega_I(I)\alpha + \beta) \\ \langle \hat{\sigma}_x \rangle(\beta|II) &= \cos(\omega_I(II)\alpha + \beta)\end{aligned}\quad (6)$$

(within the error-bars), accurately with $\omega_I(I) = 1$ and $\omega_I(II) = 0$ for the interactions strengths $\alpha = \pi/4, \pi/8$ and $\alpha = \pi/16$. The experimentally obtained values are summarized in the gray boxes under Figs. 5 - 7 and average is expressed as

$$\langle \hat{\sigma}_x \rangle(\beta) = p(I) \cos(\omega_I(I) \times \alpha + \beta) + p(II) \cos(\omega_I(II) \times \alpha + \beta) \quad (7)$$

with $p(I) = 0.8$ and $p(II) = 0.2$.

3.2 Interference context

A schematic illustration of the *interference measurement context* is given in Fig. 8 (a). The optimal correction, is given by $\beta_{\text{opt}} = -\alpha \cdot \omega_I(\pm)$, where factor $\omega_I(\pm)$ determines the average presence of the neutron in path I. In the limit $\alpha \rightarrow 0$, the path presence $\omega_I(\pm)$ converges to the weak value [4, 5]; $\beta_{\text{opt}} = -\alpha \cdot \langle \hat{\Pi}_I \rangle_w^{\psi, m\pm}$, with weak value of the path projector on to path I with initial (pre-selected) state $|\psi\rangle$ and final (post-selected) state $|m_\pm\rangle$. The respective weak values, post-selected on is an equally weighted superposition $|m_\pm\rangle = |P_x; \pm\rangle = \frac{1}{\sqrt{2}}(|P_z; +\rangle \pm |P_z; -\rangle)$, denoted as $A(m) = \frac{\langle m| \hat{A} |\psi\rangle}{\langle m| \psi\rangle} := \langle \hat{A} \rangle_w^{\psi, m}$ are obtained as $\langle \hat{\Pi}_I \rangle_w^{\psi, m+} = \frac{2}{3}$ and $\langle \hat{\Pi}_I \rangle_w^{\psi, m-} = 2$ for projectors onto path I, i. e., $\hat{A} = \hat{\Pi}_I$. Applying the respective setup from Fig. 8 (b), the system (path) state is $\hat{\rho}_S = |\psi(\chi, \gamma)\rangle \langle \psi(\chi, \gamma)|$ with $|\psi(\chi, \gamma)\rangle = \cos \frac{\gamma}{2} |P_z; +\rangle + e^{i\chi} \sin \frac{\gamma}{2} |P_z; -\rangle$ where χ is the relative phase between the eigenstates, adjusted by a phase shifter. While $\chi = 0$ accounts for the measurement results $m = +$ phase shift $\chi = \pi$ accounts for the measurement results $m = -$ (the respective phase shifts are obtained from reference measurements which is explained in detail in Appendix A).

Again we begin with measurement strength $\alpha = \pi/4$, plotted in Fig. 9. The corresponding output port probability $p(|m_+\rangle = |P_x; +\rangle, \alpha = \pi/4, |P_i\rangle) = 0.869552$ and $p(|m_-\rangle = |P_x; -\rangle, \alpha = \pi/4, |P_i\rangle) = 0.130448$. The conditional compensation fringes are shifted by $\omega_I(\pm) \alpha$, where $\omega_I(\pm)$ denotes the *average presence*

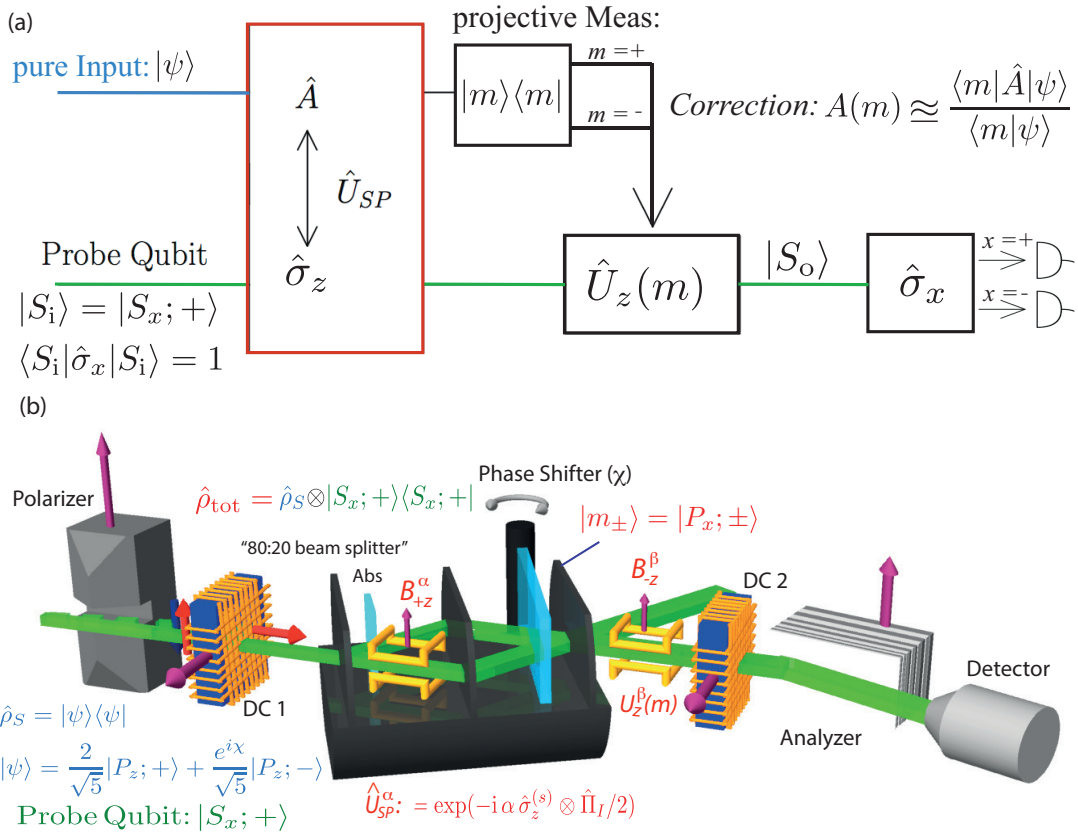


Figure 8: (a) Schematic illustration of *contextual* feedback compensation of the decoherence in a probe qubit, for projective measurements (*interference measurement context*). (b) Respective neutron interferometric setup.

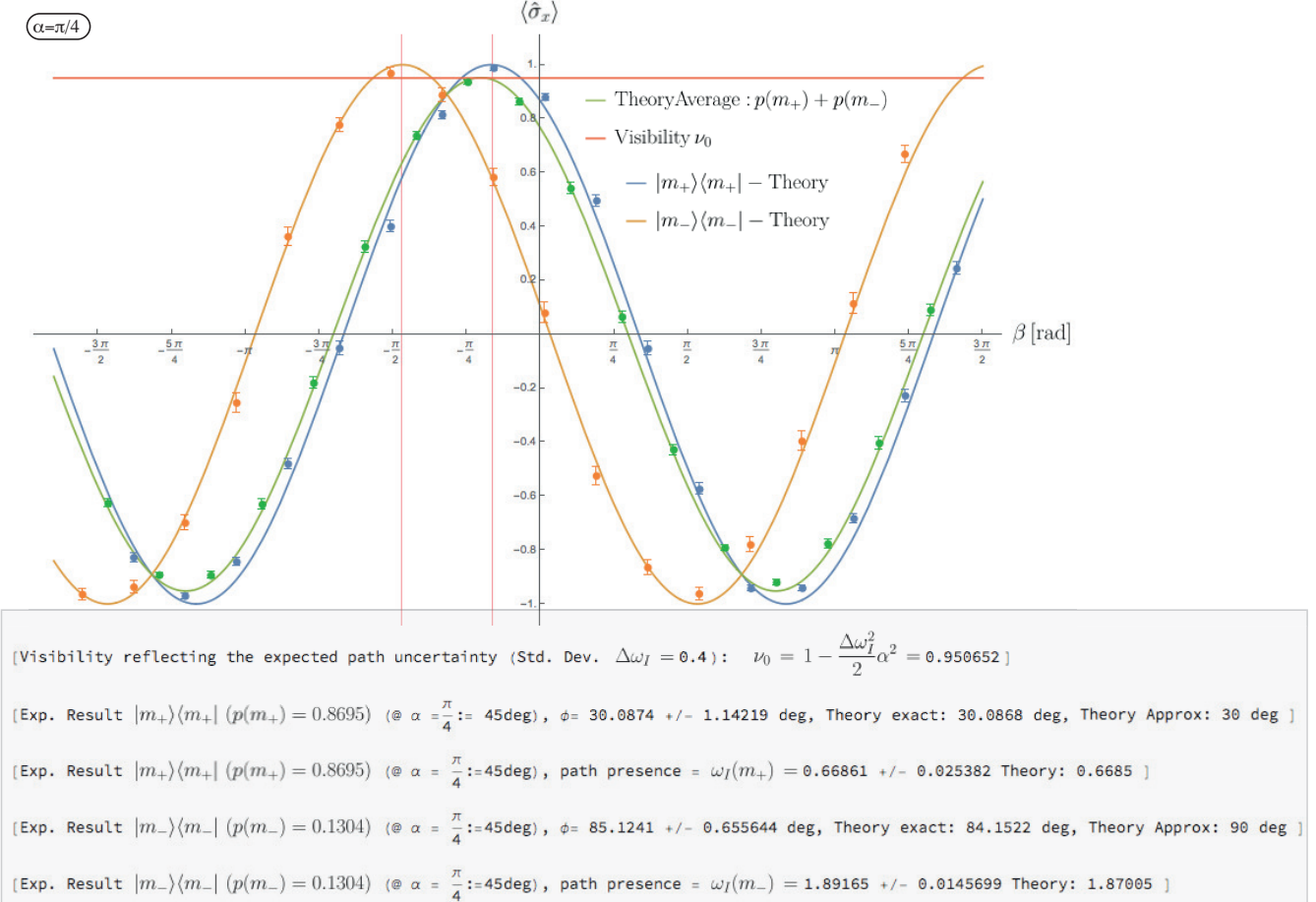


Figure 9: Experimental results of feedback compensation of the decoherence in a probe qubit, in *interference context*, for interaction strength $\alpha = \pi/4$.

of the neutron in path I, for the respective output of $m = \pm$. For $\alpha = \pi/4$ the predicted values of the path presence are $\omega_I(+)=0.668595$ and $\omega_I(-)=1.87005$ at $p(+)=0.869552$ and $p(-)=0.130448$ are evidently reproduced in the experiment, which can be seen from the values in gray box below Fig. 9. The green fringes in the figures show the statistical average of all neutrons without any output measurement of which-path information. The interference context changes the path occupation numbers to $\omega_I(+)=2/3$ and to $\omega_I(-)=2$, with probabilities of $P(+)=0.9$ and $P(-)=0.1$. For small α the experimental results converge on these values (see Fig. 10). The observable feedback fringes are approximately

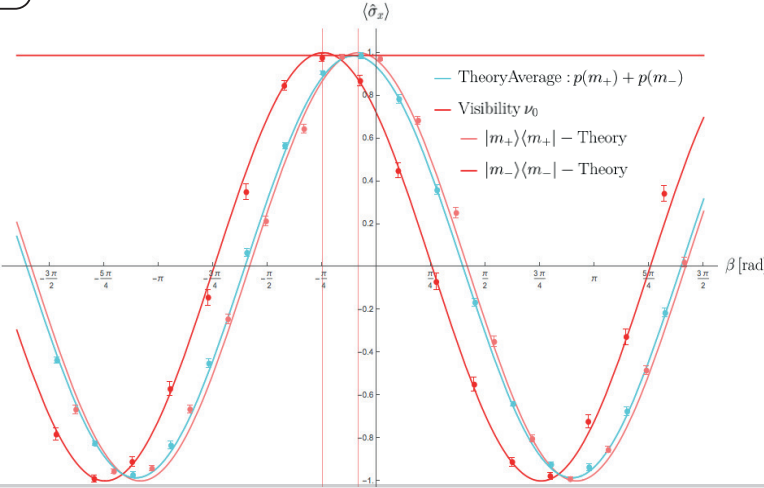
$$\begin{aligned} \langle \hat{\sigma}_x \rangle(\beta|m_+) &\approx \cos(\beta + \omega_I(+)\alpha) \\ \langle \hat{\sigma}_x \rangle(\beta|m_-) &\approx \cos(\beta + \omega_I(-)\alpha), \end{aligned} \quad (8)$$

and the average is expressed as

$$\langle \hat{\sigma}_x \rangle(\beta) = p(+) \cos(\omega_I(+)\times\alpha + \beta) + p(-) \cos(\omega_I(-)\times\alpha + \beta) \quad (9)$$

with $p(+) = 0.1$, $\omega_I(I) = 1$, $\omega_I(II) = 0$, $\omega_I(+)=2/3$ and $\omega_I(-)=2$ (see Eq. 25 from Appendix B for exact expression). Again the interaction strength α is halved to $\alpha = \pi/8$ and then halved again to $\alpha = \pi/16$, which is plotted in Fig. 10 on the next page. A plot of path presences $\omega_I(\pm)$ versus interaction strength α is given in Fig. 11.

($\alpha = \pi/8$)



[Visibility reflecting the expected path uncertainty (Std. Dev. $\Delta\omega_I = 0.4$): $\nu_0 = 1 - \frac{\Delta\omega_I^2}{2}\alpha^2 = 0.987663$]

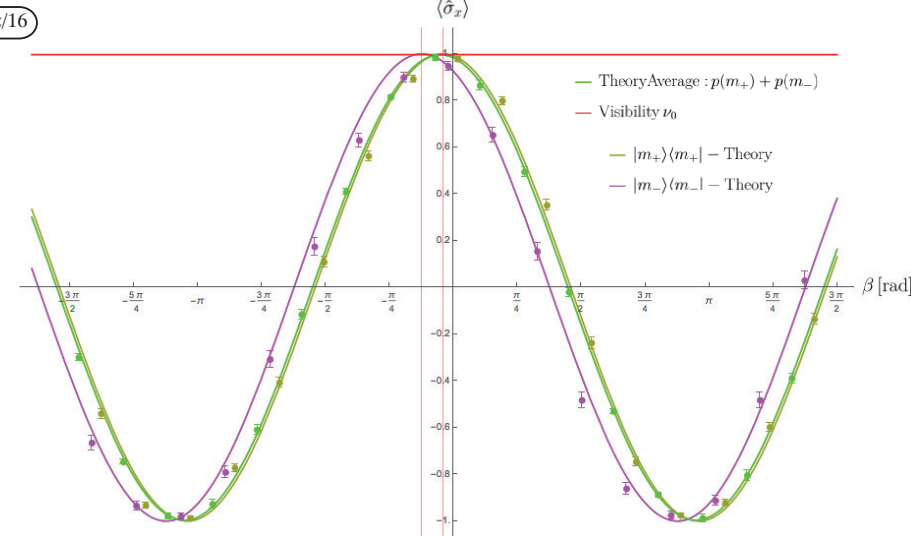
[Exp. Result $(|+m\rangle\langle+m| @ \frac{\pi}{8} := 22.5\text{deg})$, $\phi = 15.8269 +/- 1.02676 \text{ deg}$, Theory exact: 15.0107 deg , Theory Approx: 15 deg]

[Exp. Result $|m_+\rangle\langle m_+| (p(m_+) = 0.8923) (@ \alpha = \frac{\pi}{8} := 22.5\text{deg})$, path presence = $\omega_I(m_+) = 0.703417 +/- 0.0456336$ Theory: 0.6671]

[Exp. Result $(|-m\rangle\langle-m| @ \alpha = \frac{\pi}{8} := 22.5\text{deg})$, $\phi = 44.7606 +/- 0.869901 \text{ deg}$, Theory exact: 44.172 deg , Theory Approx: 45 deg]

[Exp. Result $|m_-\rangle\langle m_-| (p(m_-) = 0.1076) (@ \alpha = \frac{\pi}{8} := 22.5\text{deg})$, path presence = $\omega_I(m_-) = 1.98936 +/- 0.0386623$ Theory: 1.96320]

($\alpha = \pi/16$)



[Visibility reflecting the expected path uncertainty (Std. Dev. $\Delta\omega_I = 0.4$): $\nu_0 = 1 - \frac{\Delta\omega_I^2}{2}\alpha^2 = 0.996916$]

[Exp. Result $(|+m\rangle\langle+m| @ \frac{\pi}{16} := 11.25\text{deg})$, $\phi = 8.07702 +/- 0.986746 \text{ deg}$, Theory exact: 7.5053 deg , Theory Approx: 7.5 deg]

[Exp. Result $|m_+\rangle\langle m_+| (p(m_+) = 0.8980) (@ \alpha = \frac{\pi}{16} := 11.25\text{deg})$, path presence = $\omega_I(m_+) = 0.717957 +/- 0.0877107$ Theory: 0.66678]

[Exp. Result $(|-m\rangle\langle-m| @ \alpha = \frac{\pi}{16} := 11.25\text{deg})$, $\phi = 22.1468 +/- 0.983384 \text{ deg}$, Theory exact: 22.39285 deg , Theory Approx: 22.5 deg]

[Exp. Result $|m_-\rangle\langle m_-| (p(m_-) = 0.1019) (@ \alpha = \frac{\pi}{16} := 11.25\text{deg})$, path presence = $\omega_I(m_-) = 1.9686 +/- 0.0874119$ Theory: 1.9904]

Figure 10: Experimental results of feedback compensation of the decoherence in a probe qubit, in *interference context*, for interaction strength $\alpha = \pi/8$ and $\alpha = \pi/16$.

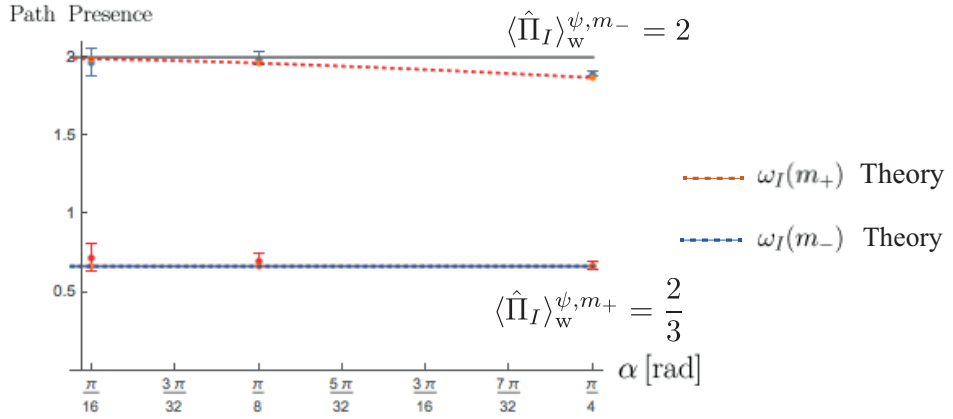


Figure 11: Path presences $\omega_I(\pm)$ versus interaction strength α . For small α the path presences converges to the respective weak values (grey lines).

Appendix A: Details of experiment, data evaluation & photos

The experiment was carried out at the neutron interferometer instrument S18 at the high-flux reactor of the Institute Laue-Langevin (ILL) in Grenoble, France. A monochromatic beam with mean wavelength $\lambda_0 = 1.91\text{\AA}$ ($\lambda/\lambda_0 \sim 0.02$) and $5 \times 7\text{mm}^2$ beam cross section is polarized by a birefringent magnetic field prism in $+z$ -direction. Owing to the angular separation at the deflection (a few seconds of arc for the parallel and anti-parallel spin state), the interferometer is adjusted so that only the spin-up component fulfills the Bragg condition at the first interferometer plate (beam splitter). After passing the magnetic field prism, the neutrons enter a static magnetic guide field which points in the $+z$ -direction. This field covers the entire setup and prevents depolarization. Before the neutron beam enters the interferometer, the neutron's spin is rotated into the x -direction by a $\pi/2$ spin-turner (DC 1). The spin turner consists of a dc coil which creates a magnetic field B_y pointing in y -direction. In this region, the spin precesses about the y -axis due to Larmor precession within dc coil. $B_y^{\pi/2}$ is adjusted such that it induces a $\pi/2$ spin rotation, thereby preparing the initial spin state $|\psi_i\rangle = |S_x; +\rangle$, representing the *probe qubit*. Entering the interferometer, the initial state of the path system (*object system*) is prepared by splitting the incident beam into two sub-beams. Behind the first plate of the interferometer, the neutron's spatial wavefunction

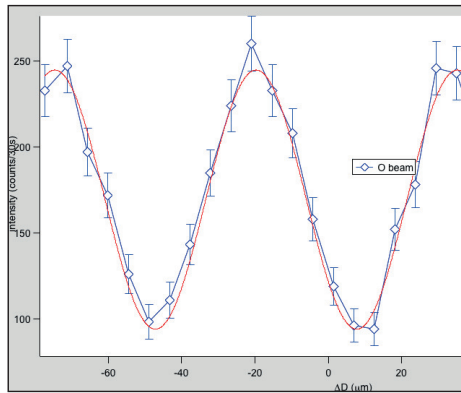


Figure 12: Typical interferogram (raw data) when rotating phase shifter flag (χ -scan).

is found in a coherent superposition of the two sub-beams belonging to path *I* and path *II*. Next, a (*weak*) spin rotations of α is introduced by local modification of the static guide field in path *I*, inducing the coupling $\hat{U}_{\text{SP}}^{\alpha}$. This is achieved by small coils aligned in a Helmholtz configuration and placed in a box which are completely flooded with temperature controlled water. The box is equipped with a tunnel so that the neutrons can pass the magnetic field region without touching any material along the beam path. As a result, the Larmor frequency is increased in path *I* by α . Before the two sub-beams are recombined at the third plate, an adjustable relative phase factor $e^{\pm i\chi/2}$ is induced by a phase shifter plate. The phase shift is given by $\chi = N_{\text{ps}} b_c \lambda D$ with atom density N_{ps} in the phase shifter plate of thickness D , the coherent scattering length b_c and the neutron wavelength λ . By rotating the phase shifter plate, χ can be tuned systematically, due to the change of the relative optical path length in path *I* and path *II*, resulting in interference fringes as plotted in Fig. 12. The phase shifter allows to select the outputs $|m_{\pm}\rangle = |P_x; \pm\rangle = \frac{1}{\sqrt{2}}(|P_z; +\rangle \pm |P_z; -\rangle)$ as maximum and minimum of the intensity oscillation respectively (reference measurement with $\alpha = 0$).

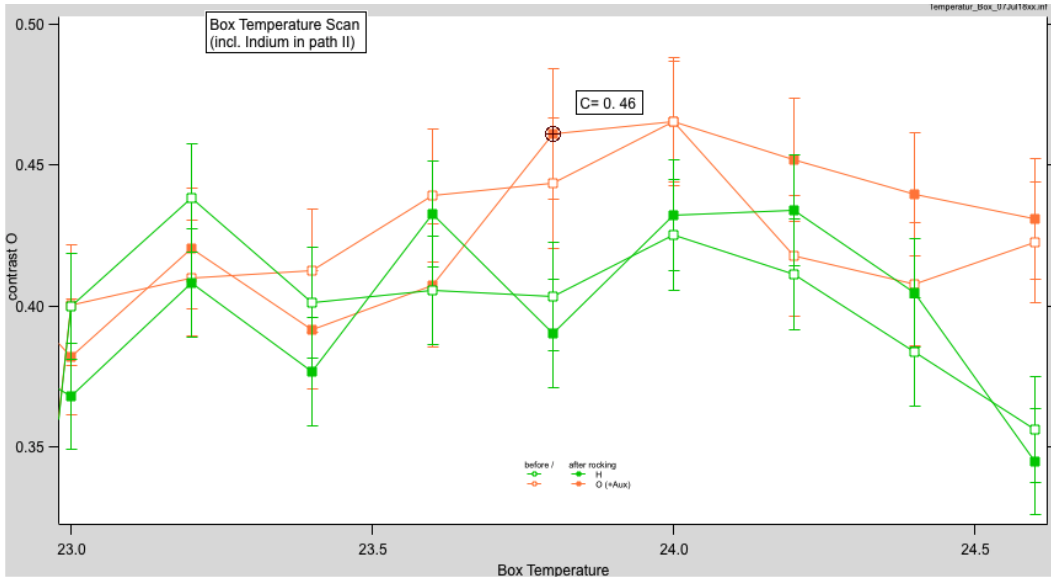


Figure 13: Temperature scans of cooling water in interferometer (α) coil.

Behind the interferometer, in the O-beam, the spin is rotated by a polar angle $\pm\pi/2$ inside a dc spin turner coil (DC 2) with accordingly adjusted static magnetic field $\pm B_y^{\pi/2}$, with accounts a spin analysis of $|\pm x\rangle\langle\pm x|$, required to calculate $\langle\hat{\sigma}_x\rangle$. In addition, DC 2 is mounted on a translation stage, depending on the position of the translation stage, the azimuthal angle β is tuned due to Larmor precession in the static magnetic guide field, which accounts for the *feedback correction operation* $\hat{U}_z^{\beta}(m)$. The spin is finally selected by a spin-dependent reflection from a bent Co-Ti supermirror array. The outgoing beam is measured using a ${}^3\text{He}$ -detector, with efficiency over 99 %. The observed average contrast (*fringe visibility*) at $\alpha = 0$ was $C_{\text{real}} = 0.46$ (see Fig. 13), which is smaller than theoretically predicted value $C_{\text{ideal}} = 0.8$ and is taken into account in the data treatment.

Since the intrinsic phase of the interferometer is very sensitive to fluctuations (both thermal and vibrational) every measurement is performed relative to a measurement with $\alpha = 0$ in *in/out style*, meaning for each phase shifter position (or β value) a measurement is done with $\alpha = 0$ and then the same position (value) with the respective value set, which is plotted in Fig. 14 (see² for complete data treatment of the experiment).

²https://www.wolframcloud.com/obj/stephan.sponar/Published/Which-Path_Context_Experimental.nb

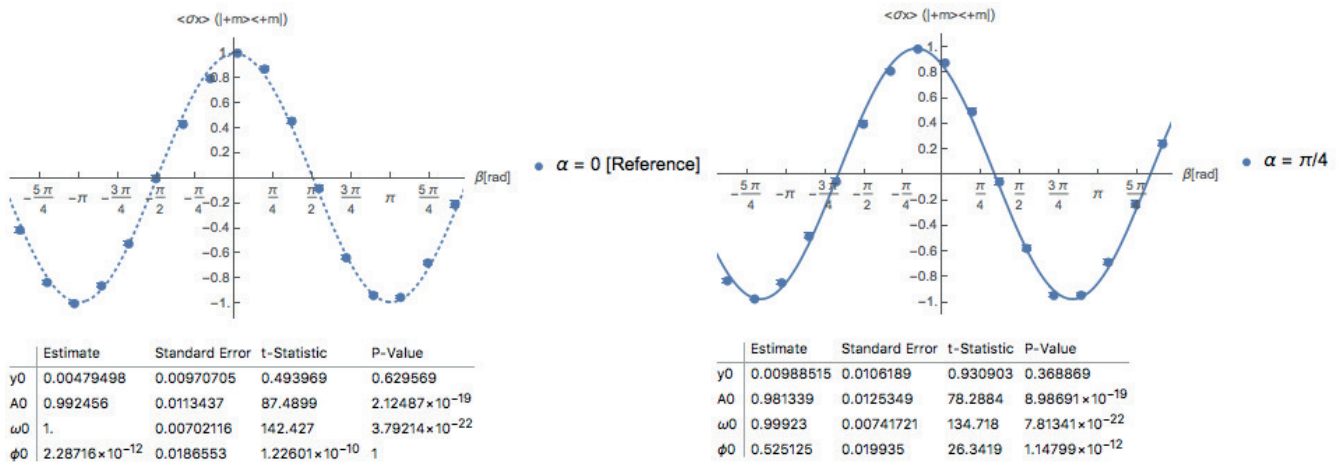


Figure 14: Relative phase measurement (β scan) with fit parameter



Figure 15: Photos of experimental setup (top) neutron interferometer detailed (bottom) from July 2021.

Appendix B: Calculation of intensities

All intensities are calculated using the following operators of the composite 2 x 2 dimensional complex Hilberspace denoted as $\mathcal{H}_{tot} = \mathcal{H}_{path} \otimes \mathcal{H}_{spin}$:

$$50:50 \text{ beam splitter: } U_B = \frac{1}{\sqrt{2}} \begin{bmatrix} 1 & 1 \\ 1 & -1 \end{bmatrix} \otimes \begin{bmatrix} 1 & 0 \\ 0 & 1 \end{bmatrix} \quad (10)$$

$$\text{Mirror: } U_M = \frac{1}{\sqrt{2}} \begin{bmatrix} 0 & 1 \\ 1 & 0 \end{bmatrix} \otimes \begin{bmatrix} 1 & 0 \\ 0 & 1 \end{bmatrix} \quad (11)$$

$$\text{Phase shifter: } U_P(\chi) = \begin{bmatrix} \text{Exp}(\frac{i\chi}{2}) & 0 \\ 0 & \text{Exp}(-\frac{i\chi}{2}) \end{bmatrix} \otimes \begin{bmatrix} 1 & 0 \\ 0 & 1 \end{bmatrix} \quad (12)$$

$$\text{Arbitrary beam splitter: } U_B(\gamma) = \frac{1}{\sqrt{2}} \begin{bmatrix} \cos \frac{\gamma}{2} & \sin \frac{\gamma}{2} \\ \sin \frac{\gamma}{2} & \cos \frac{\gamma}{2} \end{bmatrix} \otimes \begin{bmatrix} 1 & 0 \\ 0 & 1 \end{bmatrix} \quad (13)$$

$$\text{Weak coupling: } U_w(\alpha) = \begin{bmatrix} 1 & 0 \\ 0 & 0 \end{bmatrix} \otimes \begin{bmatrix} 1 & 0 \\ 0 & 1 \end{bmatrix} \cos\left(\frac{\alpha}{2}\right) - i\tilde{\sigma}\hat{a} \sin\left(\frac{\alpha}{2}\right) + \begin{bmatrix} 0 & 0 \\ 0 & 1 \end{bmatrix} \otimes \begin{bmatrix} 1 & 0 \\ 0 & 1 \end{bmatrix} \quad (14)$$

for small rotation angles α , where $\tilde{\sigma}$ is the Pauli spin operator given by $(\sigma_x, \sigma_y, \sigma_z)^T$, \hat{a} is the unit vector defining the rotation axis and α is the angel of rotation from the Larmor precession. The wavefunction just before the absorber in path II is given by

$$\rho_{\text{IFM}} = U_M \cdot U_w(\alpha) \cdot U_P(\chi) U_B(\gamma) \left(\begin{bmatrix} 1 \\ 0 \end{bmatrix} \otimes \frac{1}{\sqrt{2}} \begin{bmatrix} 1 \\ 1 \end{bmatrix} \right) U_B(\gamma)^\dagger \cdot U_P(\chi)^\dagger \cdot U_w(\alpha)^\dagger \cdot U_M^\dagger \quad (15)$$

with initial path state in + eigenstate (path I) and initial spin in x-direction $|S_i\rangle = |S_x; \pm\rangle$. The wave function behind the interferometer, including absorber, is calculated using partial trace written as

$$\rho_{\text{out}}^{(s)} = \text{Tr} \left(\hat{\Pi}_I \otimes \begin{bmatrix} 1 & 0 \\ 0 & 1 \end{bmatrix} \cdot \rho_{\text{IFM}} \right), \quad (16)$$

which is now only a single qubit system accounting for spin degree of freedom. The feedback Compensation is achieved by applying an additional spin rotation of an angle β , dependent on the measurement result of

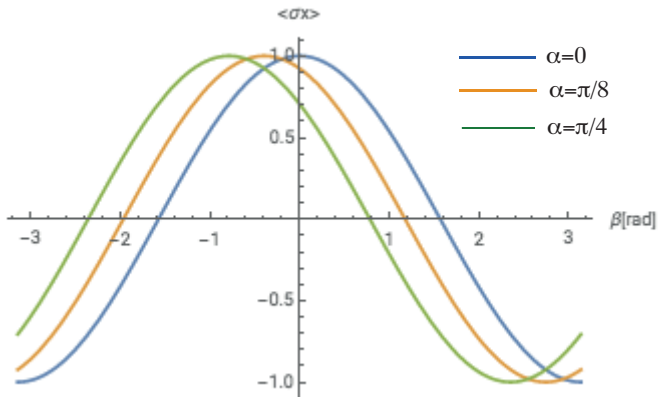


Figure 16: Feedback compensation $a = I$

$\hat{A} = \hat{\Pi}_I$, denoted as $\rho_{\text{comp}}^{(s)} = \hat{U}(\beta) \cdot \rho_{\text{out}}^{(s)} \cdot \hat{U}(\beta)^\dagger$. Finally the spin is measured in the $\pm x$ -direction yielding the following (χ -independent) results for the measurable intensities:

$$\begin{aligned} I_{+x}^{a=I} &= \cos^2\left(\frac{\beta}{2}\right) \sin^2\left(\frac{\gamma}{2}\right) \\ I_{-x}^{a=I} &= \sin^2\left(\frac{\beta}{2}\right) \sin^2\left(\frac{\gamma}{2}\right) \\ I_{+x}^{a=II} &= \cos^2\left(\frac{\alpha + \beta}{2}\right) \sin^2\left(\frac{\gamma}{2}\right) \\ I_{-x}^{a=II} &= \sin^2\left(\frac{\alpha + \beta}{2}\right) \sin^2\left(\frac{\gamma}{2}\right), \end{aligned} \tag{17}$$

and $\langle \hat{\sigma}_x \rangle(\beta|I) = \frac{I_{+x}^{a=I} - I_{-x}^{a=I}}{I_{+x}^{a=I} + I_{-x}^{a=I}} = \cos(\alpha - \beta)$ and $\langle \hat{\sigma}_x \rangle(\beta|II) = \frac{I_{+x}^{a=II} - I_{-x}^{a=II}}{I_{+x}^{a=II} + I_{-x}^{a=II}} = \cos(-\beta)$.

To get our initial state $\hat{\rho}_S = |P_i\rangle = \frac{2}{\sqrt{5}}|P_z;+\rangle + \frac{1}{\sqrt{5}}|P_z;-\rangle$, we have to set $\chi = 0$ and $\gamma = \gamma_0 := \text{ArcCos}\left((\frac{2}{\sqrt{5}})^2 - (\frac{1}{\sqrt{5}})^2\right) = \text{ArcCos}(\frac{3}{5})$. For every coupling strength α there is an optimal compensation β , where no decoherence is observed, that is $\langle \sigma_x \rangle(\text{out}) = 1$, the optimal compensation is $\beta = -\alpha$. For the results $a = II$, we simply get $\beta = 0$ (independent of α).

In the next step we change the *measurement context*; for *projective* measurements on the superposition state, with outcomes m , the feedback value $A(m)$, where $A(m)$ is given by the *weak value*, is the best estimate of A . Decoherence can be compensated completely if all weak values are fully coherent and real, as it the case for our *pure* initial (path) state

$$\hat{\rho}_S = |\psi(\chi, \gamma)\rangle\langle\psi(\chi, \gamma)| \quad \text{with} \quad |\psi(\chi, \gamma)\rangle = \cos\frac{\gamma}{2}|P_z;+\rangle + e^{i\chi}\sin\frac{\gamma}{2}|P_z;-\rangle, \tag{18}$$

with $\chi = 0$ and $\gamma = \gamma_0 := \text{ArcCos}\left((\frac{2}{\sqrt{5}})^2 - (\frac{1}{\sqrt{5}})^2\right)$, which gives

$$|\psi\rangle = \frac{2}{\sqrt{5}}|P_z;+\rangle + \frac{1}{\sqrt{5}}|P_z;-\rangle,$$

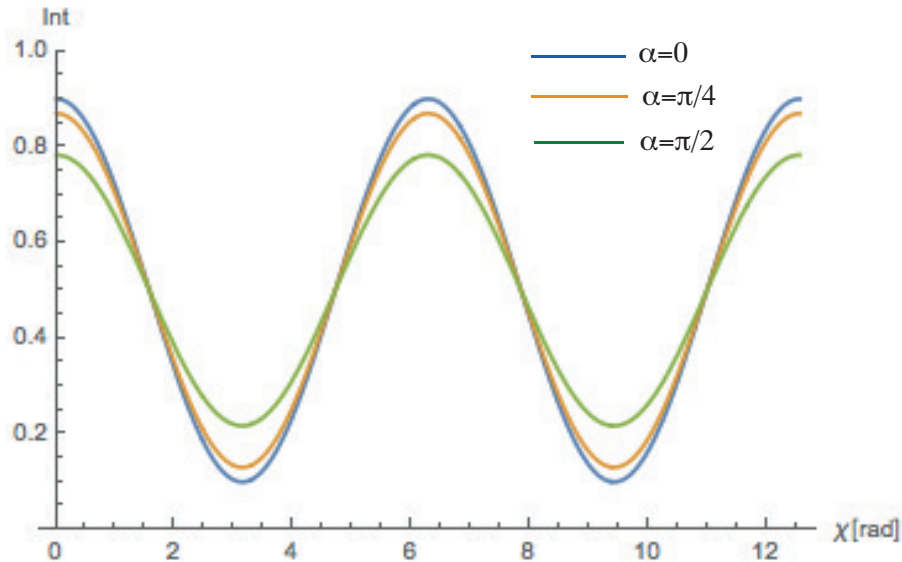


Figure 17: Intensity without feedback compensation and non spin analysis (C=0.8).

and post measurement state after *projective* measurement

$$|m_+\rangle = |P_x;+\rangle = \frac{1}{\sqrt{2}}|P_z;+\rangle + \frac{1}{\sqrt{2}}|P_z;-\rangle.$$

Applying the setup for interference measurements, the wavefunction behind the third plate of the interferometer (second beam splitter), is given by

$$\rho_{\text{out}} = U_B \cdot U_M \cdot U_w(\alpha) \cdot U_P(\chi) U_B(\gamma) \left(\begin{bmatrix} 1 \\ 0 \end{bmatrix} \otimes \frac{1}{\sqrt{2}} \begin{bmatrix} 1 \\ 1 \end{bmatrix} \right) U_B(\gamma)^\dagger \cdot U_P(\chi)^\dagger \cdot U_w(\alpha)^\dagger \cdot U_M^\dagger \cdot U_B^\dagger, \quad (19)$$

with initial path state in + eigenstate (path I) and initial spin in x-direction $|S_i\rangle = |S_x; \pm\rangle$. The wave function behind the interferometer, including absorber, is calculated using partial trace written as

$$\rho_{\text{out}}^{(s)} = \text{Tr}\left(\hat{\Pi}_I \otimes \begin{bmatrix} 1 & 0 \\ 0 & 1 \end{bmatrix} \cdot \rho_{\text{IFM}}\right), \quad (20)$$

which is now only a single qubit system accounting for spin degree of freedom. The feedback Compensation is achieved by applying an additional spin rotation of an angle β , which will be experimentally determined by searching the minimum decoherence, denoted as

$$\rho_{\text{comp}}^{(s)} = \hat{U}(\beta) \cdot \rho_{\text{out}}^{(s)} \cdot \hat{U}(\beta)^\dagger. \quad (21)$$

If no further spin analysis is performed we observe an α -dependent (measurement strength), but β -independent interference pattern denoted as

$$I_0 = \text{Tr}(\rho_{\text{comp}}^{(s)}) = \frac{1}{2} \left(1 + \cos \frac{\alpha}{2} \cos \chi \sin \gamma \right), \quad (22)$$

which illustrated in Fig. 17 for $\gamma = \gamma_0$ and three values of α versus phase shift χ . For example a spin rotation of $\alpha = \pi/4$ in path I reduces the fringe visibility of the path interference ν from $\nu(\alpha = 0) = 0.8$ to $\nu(\alpha = \pi/4) = 0.739104$. This is a reduction of a factor of 0.92388, which is $\cos(\pi/8)$, as predicted by Eq.(22).

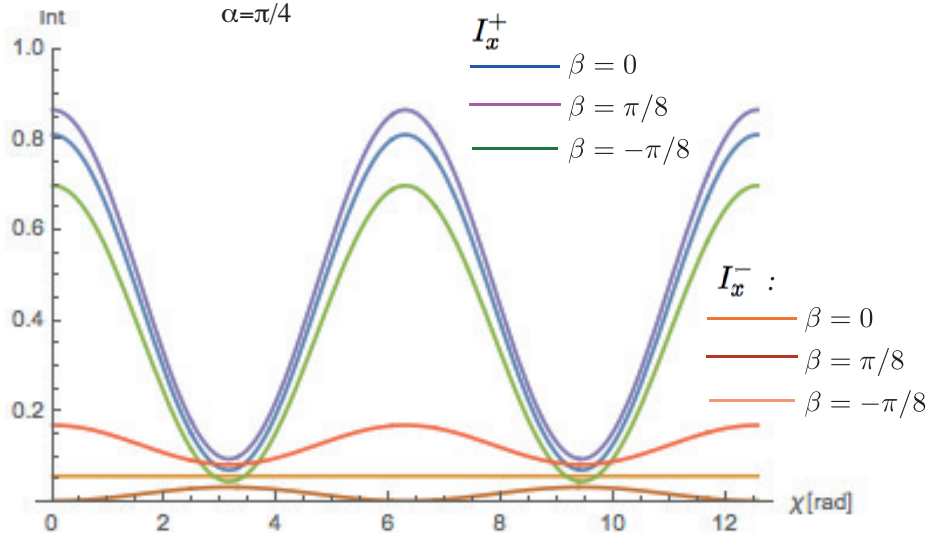


Figure 18: Intensity with feedback compensation (β) and $\pm x$ spin analysis.

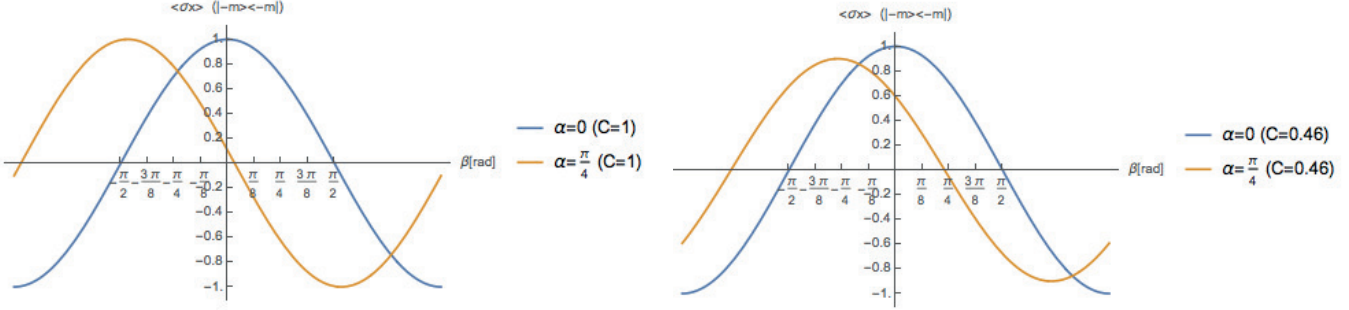


Figure 19: Intensity with $\eta = 1 \rightarrow C = 1$ (left) vs. $\eta \neq 1$ (with $C=0.46$).

The contextual feedback results in a decrease of the decoherence, denoted as $1 - \langle \hat{\sigma}_x \rangle$. Hence, the spin has to be analyzed in $\pm x$ -direction, which results in an additional β -dependence of the interference patterns:

$$\begin{aligned} I_x^+ &= \text{Tr}(\rho_{\text{comp}}^{(s)} \cdot \hat{\Pi}_{+x}^{(s)}) \\ &= \frac{1}{8} \left(2 + \cos \beta + \cos(\alpha + \beta) + 2 \cos \gamma \sin \frac{\alpha}{2} \sin \left(\frac{\alpha}{2} + \beta \right) + 2\eta \left(\cos \frac{\alpha}{2} + \cos \left(\frac{\alpha}{2} + \beta \right) \right) \cos \chi \sin \gamma \right) \end{aligned} \quad (23)$$

and

$$\begin{aligned} I_x^- &= \text{Tr}(\rho_{\text{comp}}^{(s)} \cdot \hat{\Pi}_{-x}^{(s)}) \\ &= \frac{1}{8} \left(2 - \cos \beta - \cos(\alpha + \beta) - 2 \cos \gamma \sin \frac{\alpha}{2} \sin \left(\frac{\alpha}{2} + \beta \right) + 4\eta \sin \frac{\beta}{2} \sin \left(\frac{\alpha + \beta}{2} \right) \cos \chi \sin \gamma \right), \end{aligned} \quad (24)$$

which is plotted in Fig. 18 for $\gamma = \gamma_0$, three values of β (with fixed measurement strength α and visibility $\eta = 1$) versus phase shift χ . Finally, $\langle \hat{\sigma}_x^{(s)} \rangle$ is calculated as

$$\begin{aligned} \langle \hat{\sigma}_x^{(s)} \rangle &= \frac{\text{Tr}(\rho_{\text{comp}}^{(s)} \cdot \hat{\Pi}_{+x}^{(s)}) - \text{Tr}(\rho_{\text{comp}}^{(s)} \cdot \hat{\Pi}_{-x}^{(s)})}{\text{Tr}(\rho_{\text{comp}}^{(s)})} = \frac{I_x^+ - I_x^-}{I_x^+ + I_x^-} \\ &= \frac{\cos \beta + \cos(\alpha + \beta) - 2 \cos \gamma \sin \frac{\alpha}{2} \sin \left(\frac{\alpha}{2} + \beta \right) + 2\eta \cos \left(\frac{\alpha}{2} + \beta \right) \cos \chi \sin \gamma}{2 + 2\eta \cos \frac{\alpha}{2} \cos \chi \sin \gamma}. \end{aligned} \quad (25)$$

The effect of $\eta \neq 1$ is illustrated in Fig. 19 (see ³ for Mathematica notebook with theory calculations).

³https://www.wolframcloud.com/obj/stephan.sponar/Published/Which-PathContext_Calculations.nb

References

- [1] H. F. Hofmann, Direct evaluation of measurement uncertainties by feedback compensation of decoherence, Phys. Rev. Research 3 (2021) L012011. doi:10.1103/PhysRevResearch.3.L012011.
URL <https://link.aps.org/doi/10.1103/PhysRevResearch.3.L012011>
- [2] H. Rauch, W. Treimer, U. Bonse, Test of a single crystal neutron interferometer, Phys. Lett. 47A (5) (1974) 369 – 371. doi:DOI:10.1016/0375-9601(74)90132-7.
- [3] H. Rauch, S. A. Werner, Neutron Interferometry, Clarendon Press, Oxford, 2000.
- [4] Y. Aharonov, D. Z. Albert, L. Vaidman, How the result of a measurement of a component of the spin of a spin- $1/2$ particle can turn out to be 100, Phys. Rev. Lett. 60 (1988) 1351–1354. doi:10.1103/PhysRevLett.60.1351.
URL <http://link.aps.org/doi/10.1103/PhysRevLett.60.1351>
- [5] S. Sponar, T. Denkmayr, H. Geppert, H. Lemmel, A. Matzkin, J. Tollaksen, Y. Hasegawa, Weak values obtained in matter-wave interferometry, Phys. Rev. A 92 (2015) 062121. doi:10.1103/PhysRevA.92.062121.
URL <http://link.aps.org/doi/10.1103/PhysRevA.92.062121>